SUPPLEMENTARY INFORMATION

Solar-Light-Driven Photocatalytic Water Splitting Using CuS/ZnS Type II Heterojunction: A Route to Green Hydrogen Production

Ambati Mounika Sai Krishna,[1] Kumar Babu Busi,[2] Goutam Kumar Dalapati,[3,4] Sabyasachi Chakrabortty, [2,5,]*

[1] Department of Physics, School of Engineering and Sciences (SEAS), SRM University AP, Amaravati 522240, Andhra Pradesh, India

[2] Department of Chemistry, School of Engineering and Sciences (SEAS), SRM University AP, Amaravati 522240, Andhra Pradesh, India

[3] *Center of Nanofibers and Nanotechnology, Mechanical Engineering Department, National University of Singapore – 117576.*

[4] Hydrogen Innovation Pte. Ltd., Singapore, 637141, Singapore

[5] Centre for Interdisciplinary Research, SRM University AP, Amaravati 522240, Andhra Pradesh, India

***Corresponding author:** sabyasachi.c@srmap.edu.in

1. Experimental Details

1.1 Chemicals:

All the chemical were purchased and used for the reaction without any further modification or purification. Copper (II) chloride anhydrous ($CuCl_2$ ≥98.5 to 102.00%), zinc chloride ($ZnCl_2$ – 97%), ethelene glycol (EG – $C_2H_6O_2$ ≥98%), isopropyl alcohol (IPA – C_3H_8O ≥ 99%) are purchased from Sisco Research Laboratories Pvt. Ltd. (SRL), Mumbai, Maharashtra. Sodium sulphide hydrate ($Na_2S.xH_2O$ ≥58 to 65%) was purchased from HIMEDIA Laboratories Pvt. Ltd. Mumbai, Maharashtra. Ethanol (C_2H_6O, ~99.9%) was retained from ANYTICIAL CSS REAGENT Pvt. Ltd. Na_2SO_4 is from New Material Industrial Park, Changshu city, Jiangsu. All the experiments (cleaning and washing) were conducted using Milli-Q water.

1.2 Material characterization and instrumental details:

- X-ray diffraction (XRD) analysis was performed by using Empyrean Malvern Panalytical Ltd. With a constant standby mode of XRD which has the radiation: Cu - Kα (λ = 1.54 Å) – solid photocatalyst was directly used in order to know the crystal structure and phases.
- A high-resolution transmission electron microscope (HRTEM) was characterized with JEOL-JEM 2100 instrument to capture bright field TEM images at 200 kV. Field Emission Scanning Electron Microscope (FESEM) was characterized using QUANTA 200F instrument to snap the high-resolution SEM images with an accelerating voltage of 1kV – 30kV. For electron microscope imaging, 5-10 µL of photocatalyst (2 mg diluted in 1 mL of IPA) was drop-casted on copper grid (200 mesh, from TED PELLA) – for TEM and for SEM the catalyst was drop-casted on P-type silicon glass substrate

(single side polished, diameter × thickness 3 inches × 0.5 mm from SIGMA) then all the films were dried for overnight.

- Optical absorption spectra were recorded with UV-Visible spectrophotometer (UV 2600I – Shimadzu) from 200 nm to 1400 nm wavelength by using solid powder photocatalyst.
- X-ray Photon Spectroscopy (XPS) analysis was carried out with a PHI VersaProbe III equipment using Mg Kα radiation (1253.6 eV). All the measurements were taken at a 45° detection angle, using pass energies of 55 eV (survey) and 280 eV (high-resolution). A surface area of 5 x 5 mm^2 was investigated and neutralized with a 20 μA electron flood gun. For XPS characterization, 5-10 μL of photocatalyst (2 mg diluted in 1 mL of IPA) was drop-casted on glass substrate (size 25 mm × 75 mm, from SIGMA).
- Nitrogen adsorption–desorption (BET and BJH) measurements were performed using a Quantachrome NovaWin (Nova Station A, v11.04) with a 0.05 g sample. Liquid nitrogen (MW: 28.013, density: 0.808 g/cc) was used as the adsorbate at 273 K, with a pressure tolerance of 2.000 (ads/des).
- The contact angle (surface wettability) was measured in static settings using a DMe-211 equipment from Kyowa Interface Science Co., Ltd. in Japan. Contact angle data were measured within 0-5 seconds after placing the droplet of 0.1μL and was analysed by ellipse fitting method.
- Photocatalytic tests were carried out under 1 SUN light utilizing a AAA-class solar simulator (Sciencetech, Canada) outfitted with a 300 W Xenon lamp and an AM 1.5G filter. Calibration was carried out with an SSIVT-REF silicon detector and a NIST-traceable reference cell spanning 190-1100 nm.
- Gas chromatographer (GC) was used for hydrogen quantification (produced from the photocatalyst via PC) was carried out using a Trace1310 GC (ThermoFisher Scientific)

with a RESTEK MolSieve-5A packed column. The oven was programmed from 80 °C (9 min hold) to 230 °C at 20 °C/min (3 min hold). Argon (4 mL/min) served as the carrier gas, and a thermal conductivity detector (TCD) was employed.

2. Results and discussion

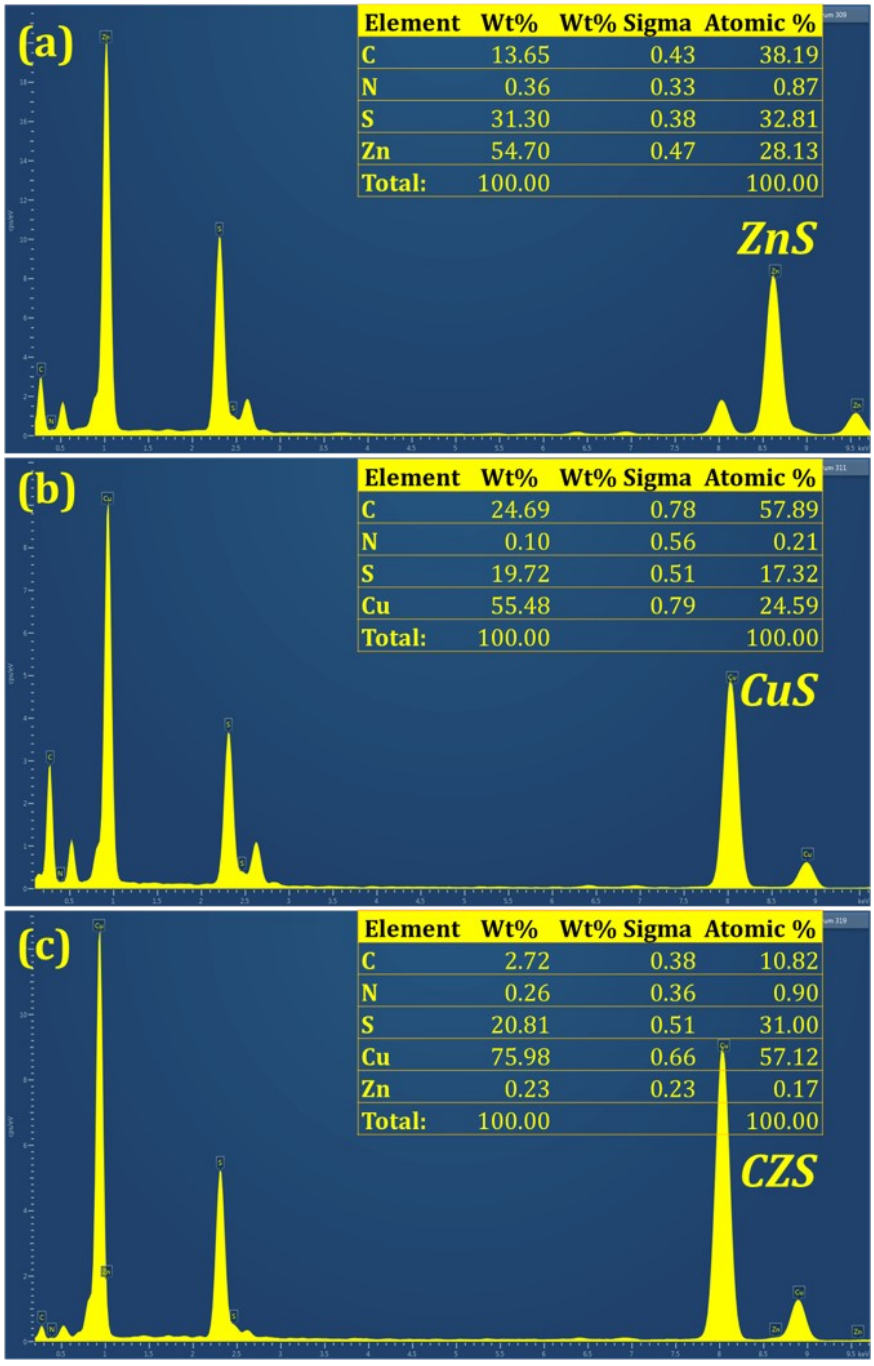

Figure S1: EDAX spectrum was captured by HRTEM images to confirm the elemental composition and the distribution within the photocatalysts: (a) bare ZnS, (b) bare CuS and (c) CZS nanocomposite.

The EDX profiles validate the presence of Zn and S in ZnS, Cu and S in CuS, and all three elements (Zn, Cu, and S) in the CZS heterostructure, confirming successful synthesis and compositional integration at the nanoscale. The elemental peaks were well-resolved with no detectable impurities, indicating high material purity.

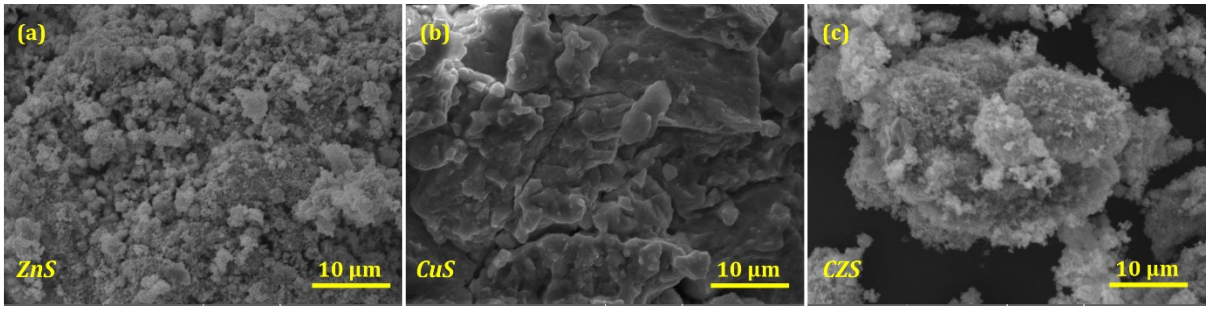

Figure S2: FESEM images were analyzed to determine surface morphology: (a) bare ZnS, (b) bare CuS, and (c) CZS heterojunction photocatalyst. FESEM of ZnS reveals an aggregated, uneven structure, whereas CuS has a more layered or flaky structure that corresponds to a plate-like crystalline. In contrast, the CZS photocatalyst has a more compact and interwoven morphology, indicating a solid integration of both ZnS and CuS phases, which is expected to enhance surface contact, charge carrier transport, and active site accessibility, all of which are critical to photocatalytic activity.

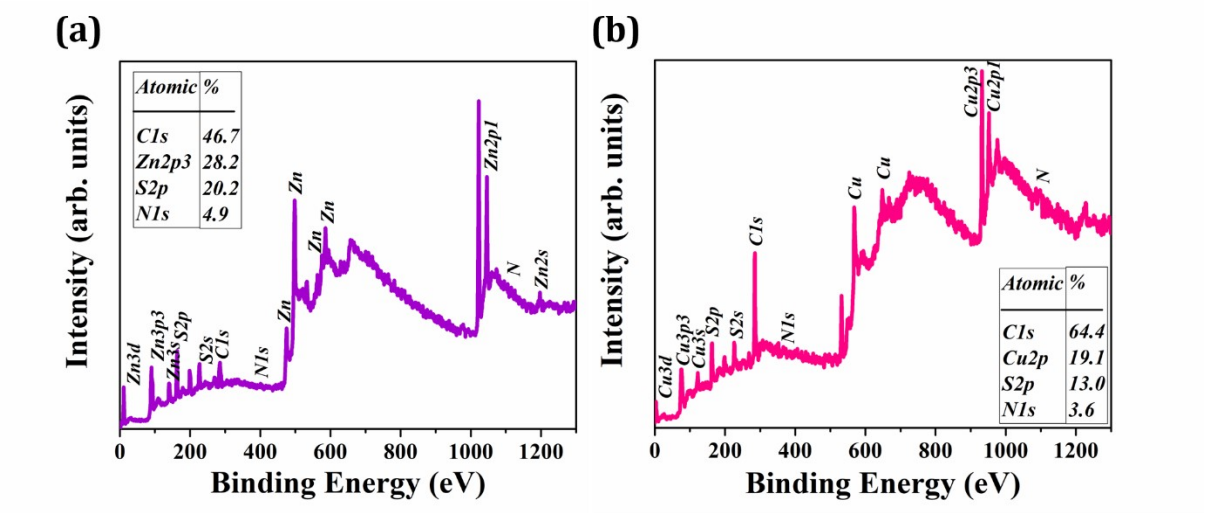

Figure S3: XPS full-scan spectra of (a) bare ZnS and (b) bare CuS photocatalysts were recorded to analyse the surface chemical composition and elemental states. These survey spectra confirm the presence of Zn, S in ZnS and Cu, S in CuS with no other impurities indicates the formation of pure phase of individual sulfide.

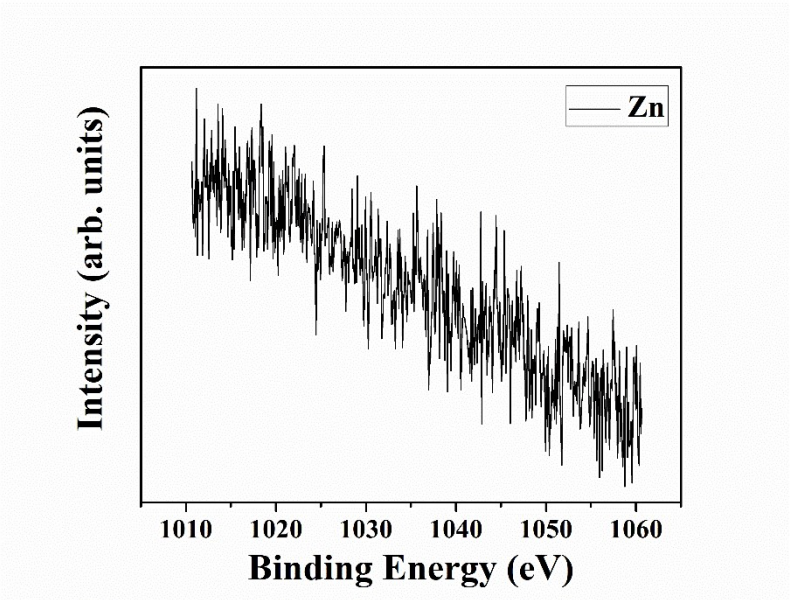

Figure S4: XPS spectrum of Zn 2p peak in CZS nanocomposite photocatalyst. Spectra show no distinct peaks of Zn $2p_{3/2}$ or Zn $2p_{1/2}$, corresponds to a low surface concentration, potentially due to subsurface distribution or low incorporation into composite and this data is also compatible with EDAX analysis.

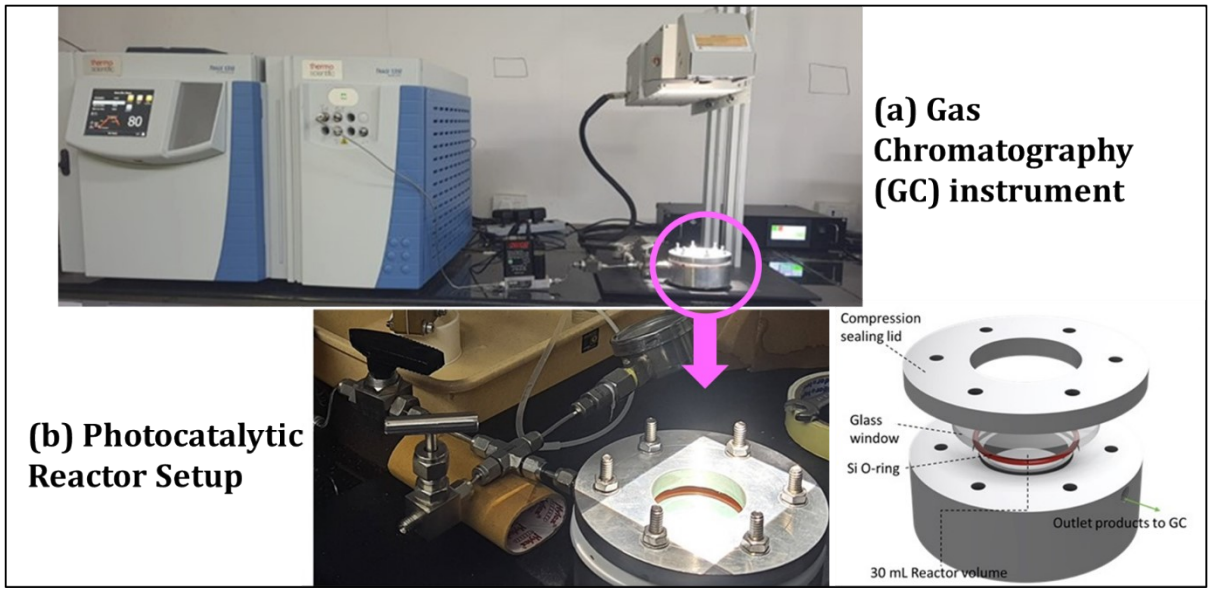

Figure S5: (a) Gas chromatography (GC) instrument set-up used for hydrogen quantification. (b) Schematic of photocatalytic reactor set-up: the reactor was sealed with the pre-dispersed photocatalyst in hole scavenger (Na_2SO_4) and placed under the solar simulator to initiate photocatalytic reaction. The evolved gases were directly connected to GC instrument for collection and quantitative analysis of H_2 production.

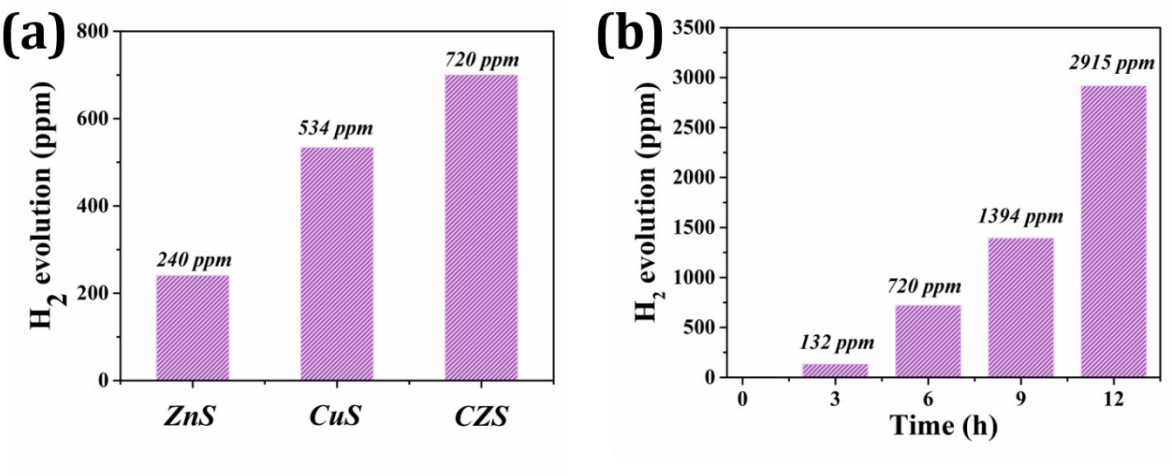

Figure S6: Amount of H_2 evolution in ppm: (a) at 6 hours irradiation of light, three photocatalyst such as bare ZnS (240 ppm), CuS (534 ppm) and CZS nanocomposite (720 ppm), highlighting the heterostructure shows the superior photocatalytic activity. (b) time-dependent H_2 evolution by CZS nanocomposite photocatalyst at 3 hours light irradiation yields 132 ppm, 720 ppm at 6 hours, 1394 ppm

at 9 hours and 2915 ppm at 12 hours irradiation of light, suggesting a sustained and enhanced H_2 evolution performance over the time via PC-WS.

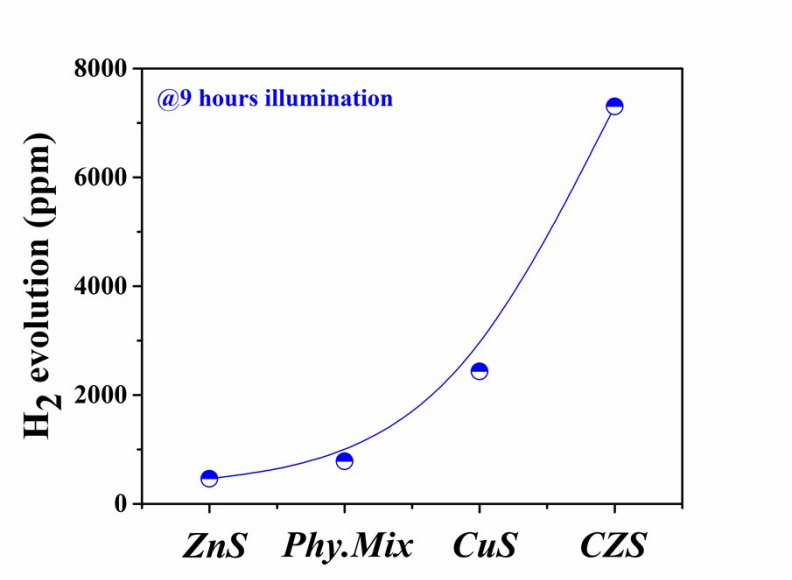

Figure S7: Amount of H_2 evolution in ppm at 9 hours light irradiation for four photocatalyst such as bare ZnS, Phy.Mix (ZnS+CuS; 1:1 ratio), CuS and CZS nanocomposite. The CZS heterostructure nanocomposite exhibits a superior photocatalytic activity compared to remaining catalysts, demonstrating the beneficial effect of heterojunction formation.

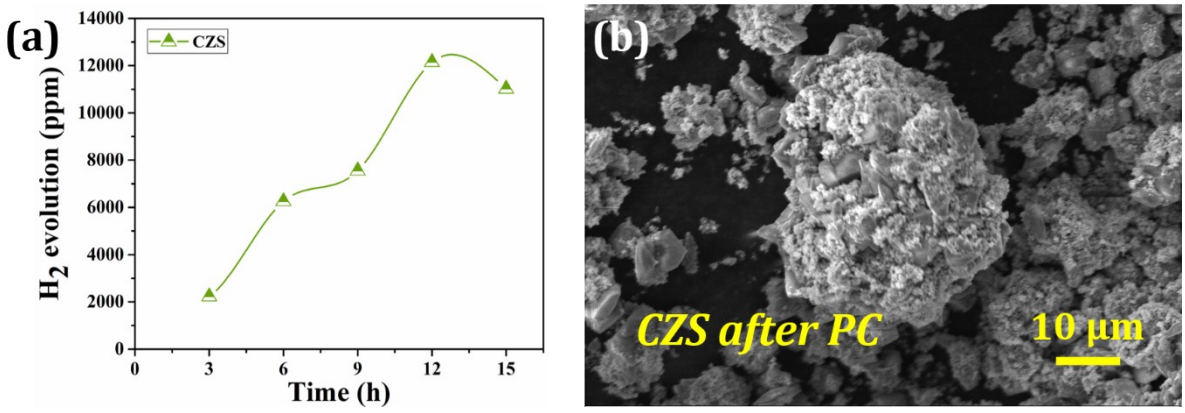

Figure S8: (a) time-dependent H_2 evolution profile of CZS nanocomposite which is recorded at every 3 hours (0, 3, 6, 9, 12, 15). A continuous illumination reveals a significant decline in the production of H_2 is observed during extended light irradiation, indicating photo-corrosion or catalyst degradation. (b) SEM image of CZS nanocomposite after the photocatalysis reaction, showing a noticeable

morphological change such as fragmentation and increased surface roughness compared to before photocatalysis reaction sample. Although some activity decay is observed under prolonged irradiation, the CZS composite demonstrates promising photocatalytic performance. But to overcome this limitation a post morphological changes after the synthesis or addition of co-catalyst or usage of other suitable hole scavengers might help.

Table S1: Calculations of the average crystalline size (nm), d-spacing (A°), stress (nm^2) and strain (ε) of bare ZnS photocatalyst.

2 theta	theta	FWHM	Crystalline (nm)	D (nm) - AVE	d-spacing (A°)	A°- AVE	Dislocation Density (nm)	nm^2 - AVE	Micro Strain (ε)	ε - AVE
28.77	14.38	3.04	2.69	3.03	3.09	2.20	137.89	113.702	51.80	34.12
48.04	24.02	3.06	2.83		1.89		124.51		30.04	
56.56	28.28	2.53	3.56		1.62		78.71		20.52	

Table S2: The average crystalline size (nm), d-spacing (A°), stress (nm^2) and strain (ε) of bare CuS photocatalyst are calculated and listed.

2 theta	theta	FWHM	Crystalline (nm)	D (nm) - AVE	d-spacing (A°)	A°- AVE	Dislocation Density (nm)	nm^2 - AVE	Micro Strain (ε)	ε - AVE
27.75	13.87	1.17	6.98	9.64	3.21	2.15	20.48	21.05	20.68	13.31
29.45	14.72	0.96	8.48		3.03		13.89		16.07	
32.42	16.21	2.10	3.93		2.75		64.58		31.55	
44.60	22.30	0.63	13.57		2.02		5.42		6.72	
48.22	24.11	0.66	13.03		1.88		5.88		6.51	
52.86	26.43	1.66	5.32		1.73		35.23		14.61	
56.40	28.20	0.43	20.76		1.63		2.31		3.53	
57.55	28.77	1.53	5.90		1.60		28.71		12.20	
59.43	29.71	1.04	8.77		1.55		12.99		7.96	

Table S3: The listed average calculations of crystalline size (nm), d-spacing (A°), stress (nm^2), and strain (ε) correspond to the CZS nanocomposite photocatalyst.

2 theta	theta	FWHM	Crystalline (nm)	D (nm) - AVE	d-spacing (A°)	A°- AVE	Dislocation Density (nm)	nm^2 - AVE	Micro Strain (ε)	ε - AVE
27.98	13.99	0.34	23.65	23.58	3.18	2.17	1.78	2.36	6.06	4.78
29.43	14.71	0.56	14.60		3.03		4.68		9.34	
32.41	16.20	0.46	17.65		2.75		3.20		7.03	
41.72	20.86	0.39	21.40		2.16		2.18		4.54	
46.47	23.23	0.34	25.29		1.95		1.56		3.47	
48.04	24.02	0.56	15.46		1.89		4.18		5.50	
55.08	27.54	0.32	27.84		1.66		1.28		2.69	
59.28	29.64	0.39	23.27		1.55		1.84		3.01	
67.76	33.88	0.22	43.08		1.38		0.53		1.44	